JET Volume 6 (2013), p.p. 31 - 46
Issue 4, November 2013

http://www.fe.um.si/sl/jet

NUMERICAL ANALYSIS OF FLOW OVER A WIND TURBINE AIRFOIL

NUMERIČNA ANALIZA TOKA OKOLI LOPATIČNEGA PROFILA VETRNE TURBINE

Janez Bitenc[ℜ], Brane Širok, Ignacijo Biluš

Keywords: wind turbine, numerical simulation, airfoil

Abstract

This work presents a comparison of flow conditions over a NACA 4421 two-dimensional airfoil with a closed trailing edge (normal airfoil shape) and a new blade shape with an open trailing edge. The numerical analysis was made using software for an approximate solution of a system of conservation law equations. The results yield a comparison of numerically obtained values of the lift coefficient, as well as diagrams of pressure coefficients and velocity vectors on the airfoil, at different angles of attack. The validity of the method of computation was confirmed with a comparison of computed lift coefficient values for the closed trailing edge profile, with experimentally acquired values from literature. It is reasonable to continue the research of flow conditions with the use of the open trailing edge airfoil.

Povzetek

Predstavljena je primerjava tokovnih razmer pri obtekanju zraka okoli dvodimenzionalnega profila NACA 4421 z zaprtim izstopnim robom (običajna oblika profila) in novo obliko lopatice z odprtim izstopnim robom. Numerična simulacija je bila narejena s programskim paketom za aproksimativno reševanje sistema parcialnih enačb, ki predstavljajo ohranitvene zakone. Rezultati podajajo primerjavo izračunanih vrednosti vzgonskih koeficientov, ter diagrame tlačnih koeficientov in vektorjev hitrosti na profilu, za različne natočne kote. Pravilnost načina izračuna je bila potrjena s primerjavo izračunanih vrednosti koeficientov vzgona za primer zaprtega

[ℜ] Corresponding author: Janez Bitenc, Tel.: +386 41 800 668, Mailing address: Ul. Janka Kača 2, SI-3310 Žalec, Slovenia
E-mail address: jbitenc@icloud.com

profila, z eksperimentalno pridobljenimi vrednostmi iz literature. Rezultati simulacij kažejo, da je smiselno nadaljevanje raziskav izboljšanja tokovnih razmer z uporabo lopatice z odprtim izstopnim robom.

1 INTRODUCTION

Wind turbines are propulsion engines for exploiting renewable energy sources. Wind turbine rotors are divided into drag-based and lift-based or horizontal and vertical, [1]. They are unable to convert the total energy from wind into mechanical work. The theoretical aerodynamic efficiency factor is called the Betz limit and is 59.3%. The motivation for these computations were the current efficiency factors with which conventional wind turbines are operating, which are much lower than the Betz limit and highly dependent on the flow conditions around airfoils.

This article discusses the airflow over wind turbine airfoils, for conventional and new blade shapes. Because different angles of attack and blade shapes lead to different flow conditions and thus significantly affect lift and drag coefficients, the discussion is limited to C_L and C_p computation for the profile in external flow. The goal was to show that the new blade type ensures more favourable flow conditions. As a new blade type, a hollow blade, [2], is introduced, with air flow streaming from the trailing edge of the profile, with which we wish to increase the lift coefficient and prevent the intrusion of secondary flow along the blade suction side in the trailing edge area. Numerical simulations of flow conditions were made with Ansys CFX software.

2 WING THEORY

The maximum obtainable power of the wind turbine in a free stream, which is independent of the design of wind turbine, is known as Betz's law. It is derived from the conservation laws of the mass and momentum of the airflow that passes through the idealized actuator disk, which extracts energy from the air stream. According to Betz's law, it is impossible for a wind turbine to take advantage of more than 59.3% of kinetic energy of the wind. In practice, wind turbines reach their peak at 75–80% of the Betz limit.

2.1 Betz limit

The Betz limit represents the ratio between the maximum achievable power of the turbine and the wind power. It equals, [3]:

$$\eta_{maks} = \frac{P_{maks}}{P_{tot}} = \frac{8}{27} \cdot 2 = 0.5926 \tag{2.1}$$

Where

$$P_{maks} = \frac{8}{27} \rho A v_{\infty}^3 \tag{2.2}$$

$$P_{tot} = \frac{1}{2} \rho A v_{\infty}^3 \tag{2.3}$$

and

$v_\infty - wind\ speed,$
$A - rotor\ disc\ area,$
$\rho - air\ density.$

Therefore, this is the maximum efficiency of wind turbines: no more than 60% of the kinetic wind energy can be converted into mechanical work, [3].

Figure 1 shows the efficiency factors of some of the practical implementations of wind turbines. On the abscissa are lined up tip speed ratios λ, representing the ratio between tip speed u and free stream airflow v_∞, [3]:

$$\lambda = \frac{u}{v_\infty} = \frac{2\pi nR}{v_\infty} \tag{2.4}$$

From the graph in Figure 1, we can see that the efficiency of wind turbine greatly depends on the tip speed ratio and rotor type. For values $\lambda < 2$, the efficiency is even in optimal conditions greatly lower than the values of $\lambda > 5$ where we obtain the maximum efficiency factors. This difference is even more obvious in actual wind turbines. The greatest efficiency factors are possible to achieve in the narrow optimal tip speed ratio interval, where the numbers range between $\eta = 0.30$ and $\eta = 0.40$, [1].

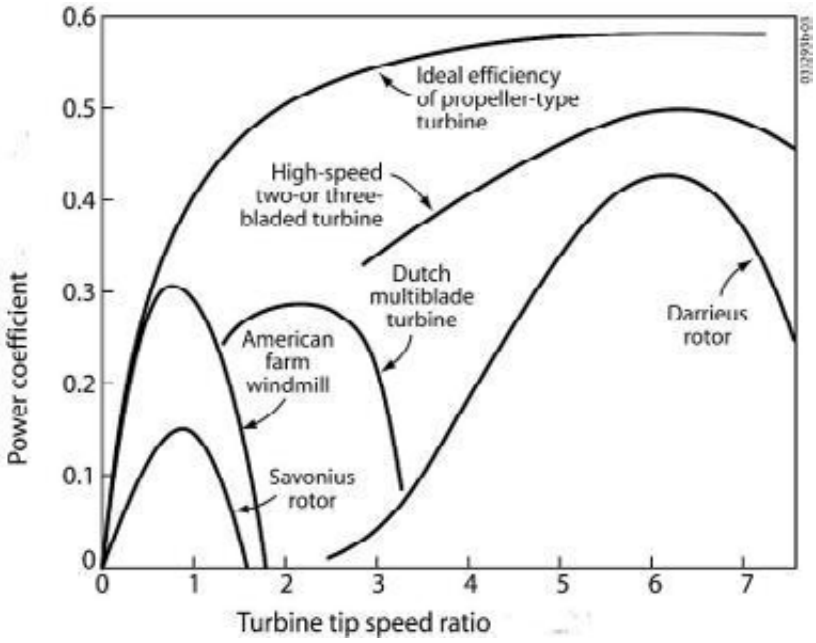

Figure 1: *Comparison of efficiency factors of some of the practical implementations of wind turbines in relation to tip speed ratio, [1]*

2.2 Aerodynamic forces and moments

Regardless of complexity of the studied model, the sources of aerodynamic forces and torque on the wing profile in the outer flow, pressure and shear stress distributions are at the airfoil. As shown in Figure 2, the pressure acts perpendicularly, and the shear stress tangentially on the surface. Shear stress is the result of friction between air and body surface, [3].

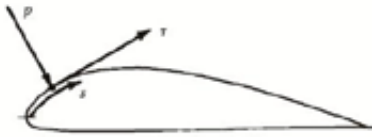

Figure 2: *Distribution of pressure p and shear stress τ along the profile, [3]*

The final effect of the distribution of p and τ, integrated over the whole body surface, is the resultant of aerodynamic forces R and momentum M on the body, as shown in Figure 3.

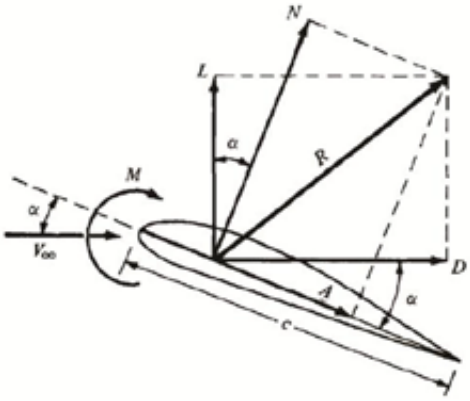

Figure 3: *Resultant of aerodynamic forces on the profile, its components and momentum*

The resultant forces R can be divided into components; two pairs are represented in Figure 3. Speed v_∞ is the free stream speed.

In Figure 3, by definition, the marked forces are, [3]

L is lift force. It is the component of resultant force R, perpendicular to v_∞

D is drag force. It is the component of resultant force R, parallel to v_∞

N is normal force. It is the component of resultant force R, perpendicular to c

A is axial force. It is the component of resultant force R, parallel to c

The relation between L and N, as well as D and A gives the equations [3]

$$L = N\cos\alpha - A\sin\alpha \tag{2.5}$$

$$D = N\sin\alpha - A\cos\alpha \tag{2.6}$$

2.3 Dimensionless coefficients

Lift force is the result of change in the momentum of the air as it streams onto the blade. Drag force is the result of friction and pressure differences. Usually, they are represented with lift C_L and drag coefficients C_D,[1]

$$C_L = \frac{L}{\frac{1}{2} v_\infty^2 \rho_\infty S} \tag{2.7}$$

$$C_D = \frac{D}{\frac{1}{2} v_\infty^2 \rho_\infty S} \tag{2.8}$$

where L and D are lift and drag forces (Equations 2.5 and 2.6), v_∞ flow velocity and S wing area. Both coefficients are dependent on flow conditions, which are primarily determined by the angle of incidence α, [1].

Another influential dimensionless coefficient is the pressure coefficient C_p

$$C_p = \frac{p_\infty}{\frac{1}{2} v_\infty^2 \rho_\infty} \tag{2.9}$$

2.4 Flow separation and the impact on the lift coefficient

With increasing air velocity or increasing values of the Reynolds number, the boundary layer along the profile changes. Speed distribution in the boundary layer is dependent on shear forces τ, acting along the wall (Figure 4).

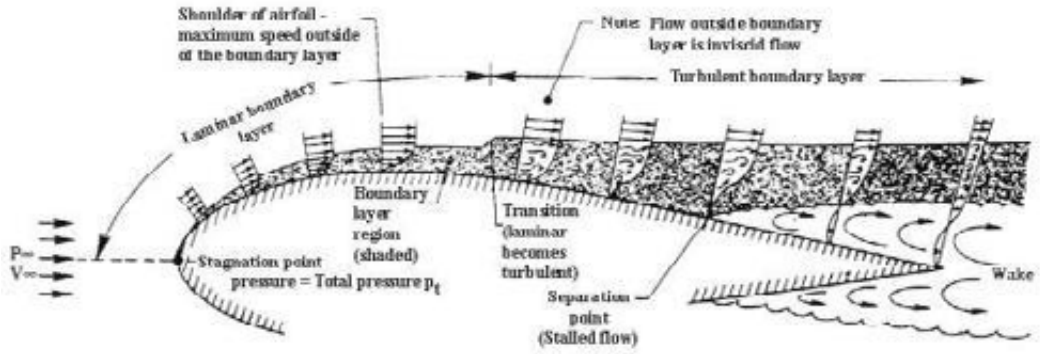

Figure 4: *Development of boundary layer along the wing profile, [4]*

The boundary layer is initially laminar, but depending on the Reynolds number and angle of attack α, it becomes unstable at a certain distance from the leading edge, where it develops into turbulent boundary layer. The effect of pressure gradient on the boundary layer is evident from Figure 4. Downstream, it has enormous impact on flow conditions along the wall and thus on the flow separation. Velocity increases behind the leading edge, where the profile widens. In contrast, the velocity lowers in the area of profile narrowing. Consequently, on the front of the profile the pressure lowers and increases towards the trailing edge, [5].

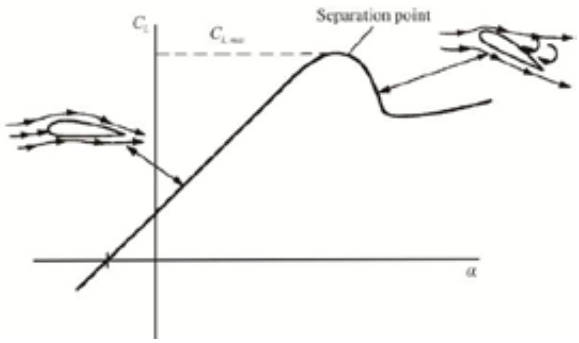

Figure 5: *Example of lift coefficient change in relation to angle of attack, [3]*

The lift coefficient increases linearly until a critical angle is reached and the maximum lift coefficient is achieved. The point at which tearing of the boundary layer and flow swirling occurs is called the flow separation point. At that moment, the lift coefficient suddenly drops and the lift force collapses (Figure 5), [3].

The purpose of this study was to analyse the impact of the new blade shape on the flow separation point and consequently on the airfoil lift coefficient.

3 NUMERICAL SIMULATION

3.1 The governing equations

The numerical simulation was made using RANS (Reynolds Averaged Navier-Stokes) method combined with the two equation turbulence model. The governing equations are:

- continuity equation

$$\boldsymbol{\nabla} \cdot \boldsymbol{U} = \frac{1}{\rho} \dot{m} \tag{3.1}$$

- momentum equation

$$\frac{\partial(\rho \boldsymbol{U})}{\partial t} + \boldsymbol{\nabla} \cdot (\rho \boldsymbol{U}\boldsymbol{U}) = -\boldsymbol{\nabla} P + \boldsymbol{\nabla} \cdot \tau + S_M \tag{3.2}$$

In the equation system above, $\boldsymbol{U}$ $[\mathrm{m/s}]$ represents the time averaged mixture velocity, P $[\mathrm{Pa}]$ is the time averaged pressure, ρ $[\mathrm{kg/m^3}]$ is density, τ $[\mathrm{N/m^2}]$ is stress tensor and S_M $[\mathrm{kg/m^2 s^2}]$ are momentum sources.

In order to close the set of governing equations, additional modelling is required to compute the turbulence quantities. The turbulence quantities were modelled using a conventional *SST* model.

3.2 Geometry and meshing

NACA 4421 profile, [6], was used for the computation for different angles of attack α. Meshing was conducted with ANSYS ICEM software. The domain is rectangular in shape and shown in Figure 6. The main dimensions, rounded to the nearest whole number, are:

- Domain length is 6.7201·c [m],
- domain height is 3.3036·c [m],
- distance from the profile leading edge to front wall of the domain is 1.6518·c [m].

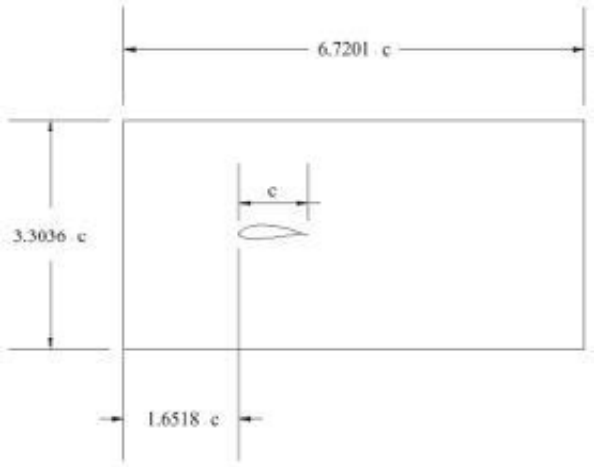

Figure 6: *Domain and profile dimensions in meters [m]*

Two numerical analyses of flow over closed and open trailing edge profiles were made. In the first, data from the literature have been used, [6]. The chord lengths c are:

- chord length of closed trailing edge profile is c = 3.027 m,
- chord length of open trailing edge profile is c = 2.927 m.

In second, the angle of attack was fixed at α = 3° and the analysis was made for three different domain inlet and profile outlet velocities, [7].

Chord lengths c are:

- chord length of closed trailing edge profile is c = 0.03027 m,
- chord length of open trailing edge profile is c = 0.02927 m.

To determine the appropriate mesh, a nodal analysis was made. Three mesh densities were made, for four angles of attack. The obtained results were compared with experimental ones [6]. The middle mesh density was chosen; the details of it are:

- number of nodes: 176,000,
- number of elements: 87,000.

3.3 Numerical simulation parameters

For the computation of wind turbine airfoil characteristics, a steady-state simulation was used. A graph of experimentally obtained lift coefficient values for the Reynolds number of $3 \cdot 10^6$ was used as a reference data, [6].

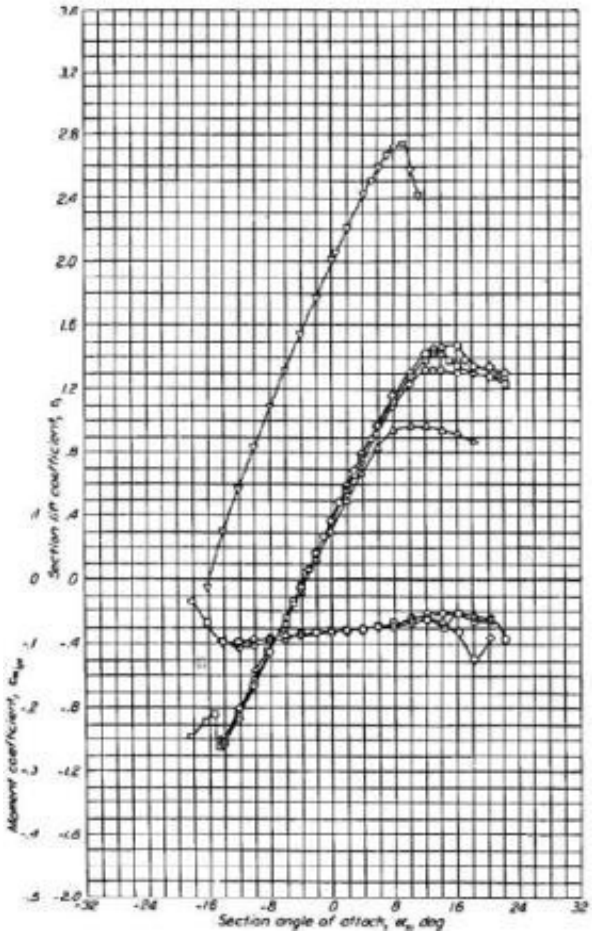

Figure 7: *NACA 4421 lift coefficients; "o" indicates results at Re = 3.0· 106, [6]*

The outlet velocity on the trailing edge of an opened profile was 12 m/s. The fluid used was air at a temperature of 25° C and ambient pressure of 101325 Pa. Due to potential reversed vortices, the outlet edge of the domain was defined as "opening", at a pressure of 0 Pa. The upper and lower sides of the domain, as well as suction and pressure sides of the profile, were defined as a "no-slip wall". Boundary conditions are shown in Figure 8. The SST turbulent model was used, which provides more accurate results about events along the wall, due to its properties.

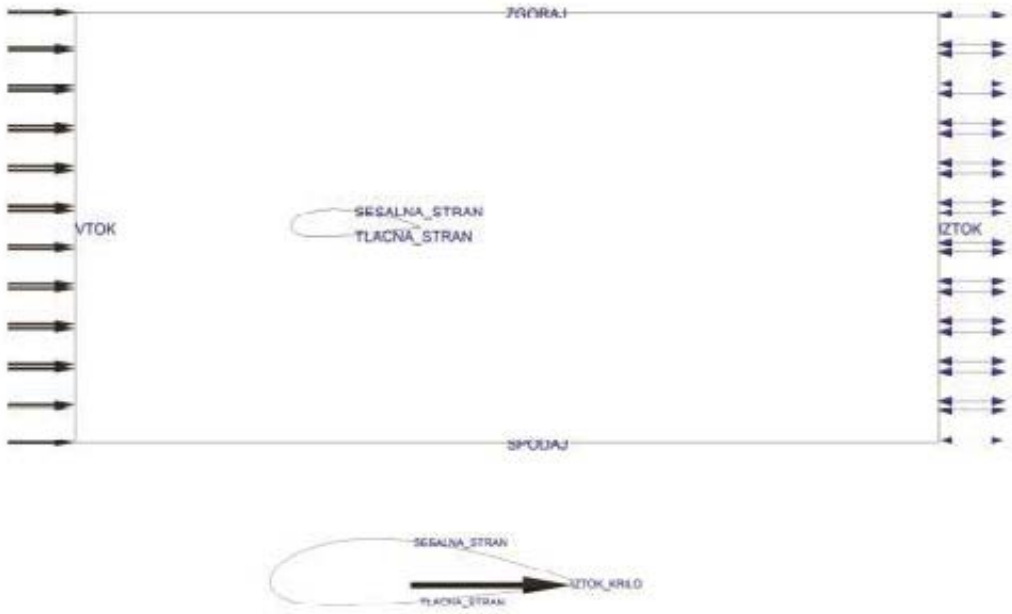

Figure 8: *Boundary conditions for closed trailing edge (above) and open trailing edge profile (below). Domain boundary conditions are in both cases the same*

At a α = 3° angle of attack, a numerical analysis of flow for the closed and open trailing edge profile was made at three different inlet and outlet velocities. Inlet velocity was defined in the form of a developed flow profile. The open trailing edge outlet velocity v_i, was determined as a value of speed function at the point y = -0.035 (maximal velocity) and reduced by a certain percentage.

4 RESULTS AND DISCUSSION

4.1 Comparison of lift coefficients

The computed data was compared with experimentally obtained values of C_L, [6], shown in Figure 7.

Figure 9 presents the comparison of computed values of C_L for both types of profiles, with the experimentally obtained values.

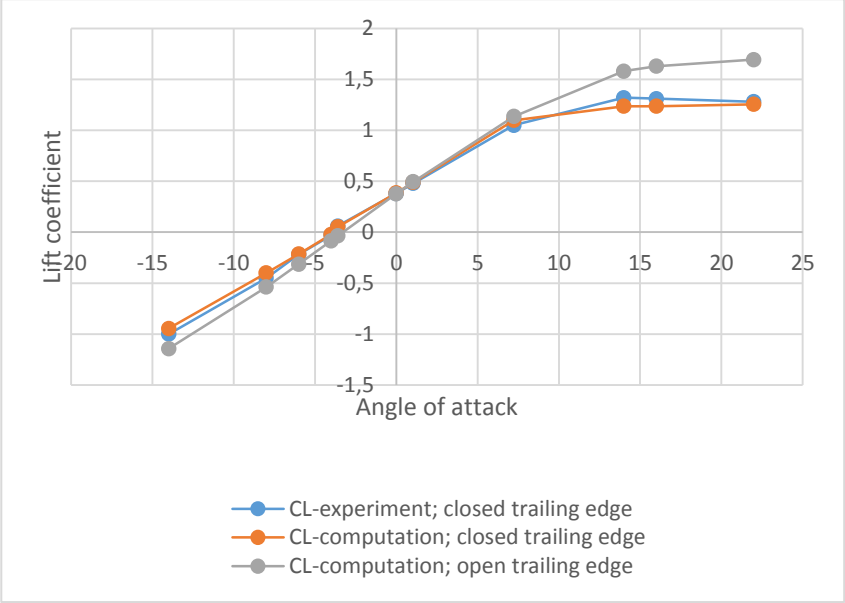

Figure 9: *Comparison of lift coefficients*

Good correlation of experimental and computed values for basic profile (closed trailing edge profile) is evident from the diagram above, as well as increase of lift coefficient in the case of an open trailing edge profile.

4.2 Comparison of pressure coefficients

In Figures 10 to 13, comparisons of pressure coefficient C_p and shear stress for both types of profiles are given, at angles of attack $\alpha = 7.24°$ and $\alpha = 14°$.

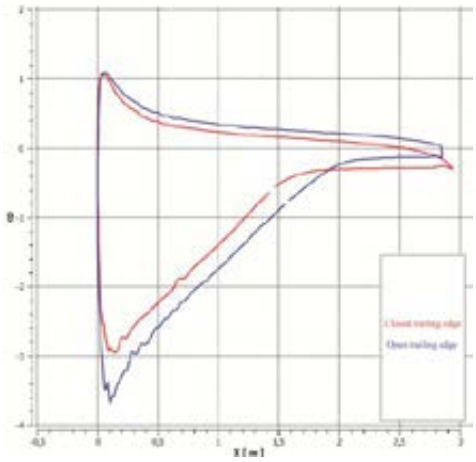

Figure 10: *Pressure coefficient; α = 14°*

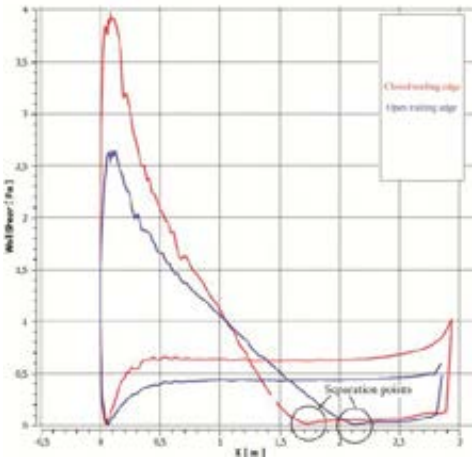

Figure 11: *Shear stress; α = 14°*

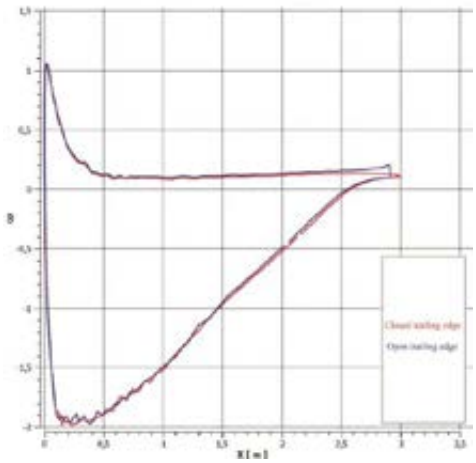

Figure 12: *Pressure coefficient; α = 7.24°*

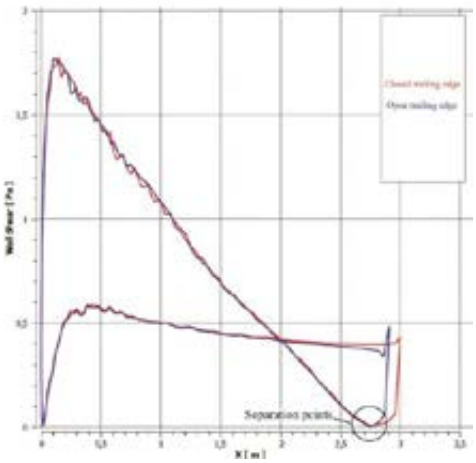

Figure 13: *Shear stress; α = 7.24°*

From Figures 10 and 12, it is evident that the negative values of pressure coefficient present greater lift force, because the lowering of the pressure on the suction side means a greater pressure difference. Separation points are evident from Figures 11 and 13, in which the shear force equals zero. At absolute values of separation points, the shortening of the blade because of a cut trailing edge needs to be taken into account.

Figure 14 shows velocity vectors at angles of attack 14° and 7.24°. A later beginning of flow swirling at the open trailing edge profile is evident, which indicates a movement of the separation point towards the trailing edge of the profile.

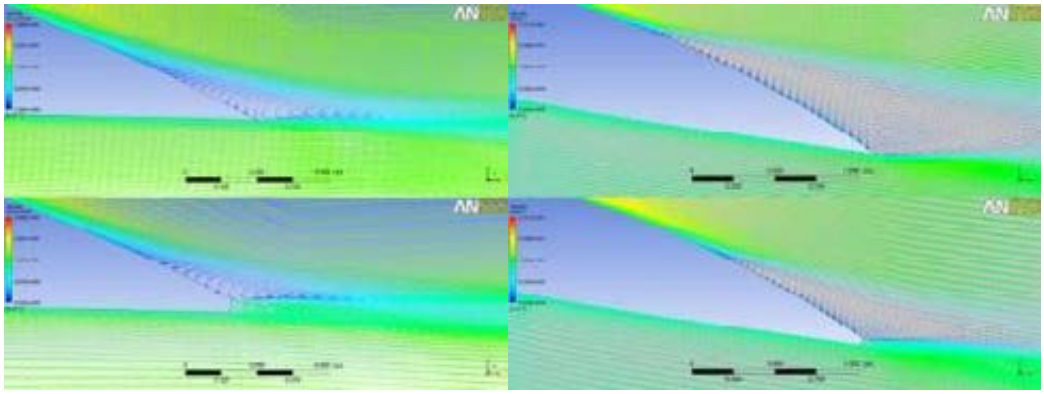

(a) (b)

Figure 14: *Comparison of velocity vectors along the profile at angles of attack α = 14° (a) and α = 7.24° (b)*

4.3 Impact of air velocity change on the results

In Table 1 and in Figure 15 andFigure 16, the results of numerical analysis for closed and open trailing edge profiles, at an angle of attack of 3° and three different inlet and outlet air velocities are shown.

Table 1: *C_L at angle of attack α = 3°*

	Velocity v_1	Velocity v_2	Velocity v_3
C_L for closed trailing edge profile	0.0486	0.0495	0.0504
C_L for open trailing edge profile	0.0856	0.0916	0.0963

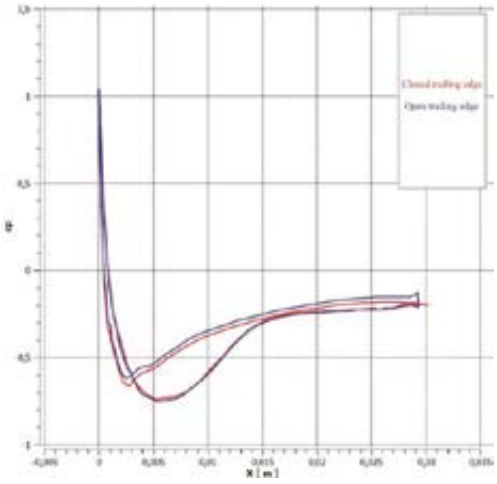

Figure 15: *Pressure coefficient at air velocity v_1 and angle of attack α = 3°*

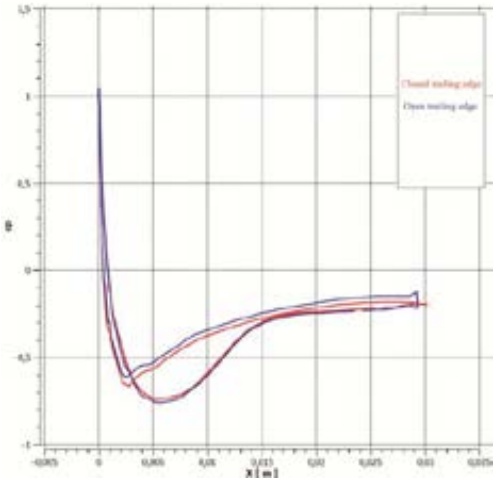

Figure 16: *Pressure coefficient at air velocity v_3 and angle of attack α = 3°*

From the results, it is evident that lift coefficients are raised in accordance to velocity. The difference between C_L for closed and open trailing edge profile is not the same, but rises with the rising of the velocity. Figure 15 and Figure 16 show the comparison of pressure coefficients of close and open trailing edge profiles. Because of the small values of C_L, differences between C_p are barely noticeable.

5 DISCUSSION

The end results of the numerical analysis of flow over wind turbine airfoil indicate an improvement of flow conditions in case of open trailing edge airfoil, for angles of attack of $\alpha > 0°$. At angles $\alpha \leq 0°$, the lift coefficients deteriorate, because of the flipped flow conditions on the suction and pressure sides.

The values of lift coefficient for closed and open trailing edge profiles give the typical lift coefficient distribution, which raises linearly with an increasing angle of attack and begins to drop when a critical angle of attack is attained. From the presented figures, it is clear that the computationally obtained values correlate well with experimental data. Later flow separation is evident in the case of the open trailing edge profile, especially at greater angles of attack. The average percentage of lift coefficient increase in case of the new blade type is (for the discussed angles of attack greater than 0°): approximately 15%. The results of the numerical analysis at an angle of attack of 3° and three different velocities showed that with proportional increases of air velocity at the domain inlet and the open trailing edge outlet, lift coefficient also increases. C_L in case of open trailing edge profile is on average 52% greater than in case of closed trailing edge profile.

Given the above, we can conclude that the open trailing edge profile favourably impacts flow conditions.

---

6 CONCLUSIONS

At default simplifications (2D model, stationery flow field, ignoring the kinetic energy of flow through the open trailing edge on the C_L formula), it was found that the open edge profile favourably impacts C_L and C_p for positive values of angle α.

The use of CFX software for analysis of airflow over wind turbine airfoil was shown to be appropriate. Such a way of studying flow conditions is cheaper, but nevertheless presents an experiment an essential tool for the validation of computations and understanding the dynamics of the phenomenon.

The improvement of numerically computed lift coefficients in the case of an open trailing edge airfoil may seem highly significant, but it is necessary to take into account that it is just a two-dimensional numerical computation, for which no kinetic energy necessary for flow through open trailing edge of the profile was incorporated. Thus, a possibility for further research of flow conditions is offered, taking account of three dimensions, a greater number of blades, the rotation of the rotor and the changing angle of attack across the blade into account.

It would be intriguing to see how that kind of blade would behave in a laboratory experiment, from which a more realistic picture and validation of the assumed hypothesis could be obtained.

References

[1] **A. Hribernik**: *Obnovljivi viri energije*, Maribor: Založništvo Fakultete za strojništvo, 2010.
[2] **M. Eberlinc, B. Širok and M. Hočevar**: *"Patented Hollow Blades of the Axial Fan with Trailing Edge Self-Induced Blowing"* Recent Patents on Mechanical Engineering, vol. 2, no. 1, pp. 1–7, 2009.
[3] **J. D. Anderson**: *Fundamentals of aerodynamics*, 3rd ed., New York: McGraw-Hill, 2001.
[4] **Aerospace engineering***: "Aerospace engineering"* February 2013. [Online]. Available: http://aerospaceengineeringblog.com/bio-mimetic-drag-reduction-2/.
[5] **M. Fike**: *Eksperimentalna in numerična raziskava tokovnih pojavov v aksialnem ventilatorju*, Maribor: Fakulteta za strojništvo, 2013.
[6] **I. H. Abbott and A. E. Von Doenhoff**: *Theory of wing sections*, Canada: General Publishing Company, 1959.
[7] **M. Eberlinc, B. Širok, M. Dular and M. Hočevar**: *"Modification of axial fan flow by trailing edge self-induced blowing"* Journal of Fluids Engineering, vol. 131, November 2009.
[8] ANSYS, Help, 14.0 ed., 2011.
[9] **T. Burton, N. Jenkins, S. David and E. Bossanyi**: *Wind energy handbook*, 2 ed., United Kingdom: John Wiley & Sons, Ltd., 2011.
[10] **E. L. Houghton and P. W. Carpenter**: *Aerodynamics for engineering students*, 5 ed., Butterworth-Heineman, 2003.
[11] **M. Malgaj**: *"Obnovljivi viri v EU in položaj Slovenije"* February 2013. [Online]. Available: http://www.zelenaslovenija.si/images/stories/pdf_dokumenti/Obnovljivi-viri-energije-v-Sloveniji.pdf.
[12] **A. Predin**: *Vetrne turbine*, Maribor, 2011.

Nomenclature

(Symbols)	(Symbol meaning)
A	Area
A	axial force
C_L	lift coefficient
C_D	drag coefficient
c	chord length
D	drag force
F_x	axial force
L	lift force
l	characteristic length
M	Torque
$\dot{m}$	mass flow rate
N	normal force
P_{tot}	airstream power
P	Power
P_{maks}	maximum power
p_∞	upstream pressure
p	Pressure
R	resultant of aerodynamic forces
S	reference area
S_M	momentum sources
t	Time
u	tangential velocity
U	time averaged mixture velocity
v_∞	free stream velocity
α	angle of attack
η_{maks}	maximum coefficient
λ	tip speed ratio
ν	kinematic viscosity
ρ_∞	free stream air density
τ	shear stress; stress tensor